![AIAA logo]

AIAA-2002-0419
Reynolds Number and Leading-Edge Bluntness Effects on a 65° Delta Wing

J. M. Luckring
NASA Langley Research Center
Hampton, Virginia

40th AIAA Aerospace Sciences Meeting & Exhibit
14-17 January 2002
Reno, Nevada

Reynolds Number and Leading-Edge Bluntness Effects on a 65° Delta Wing

J. M. Luckring*
Aerodynamics, Aerothermodynamics, and Acoustics Competency
NASA Langley Research Center
Hampton, Virginia

ABSTRACT
A 65° delta wing has been tested in the National Transonic Facility (NTF) at mean aerodynamic chord Reynolds numbers from 6 million to 120 million at subsonic and transonic speeds. The configuration incorporated systematic variation of the leading edge bluntness. The analysis for this paper is focused on the Reynolds number and bluntness effects at subsonic speeds (M = 0.4) from this data set. The results show significant effects of both these parameters on the onset and progression of leading-edge vortex separation.

NOMENCLATURE

AR	wing aspect ratio, 1.8652
b_{le}	leading-edge bluntness, r_{le}/c_{bar}
b/2	wing semispan, 1.0 ft.
C_m	pitching moment coefficient about $0.25c_{bar}$
C_N	normal force coefficient
C_p	pressure coefficient
c	wing chord
c_{bar}	wing mean aerodynamic chord, 1.4297 ft.
c_r	wing root chord, 2.1445 ft.
c_t	wing tip chord, 0 ft.
d	sting diameter, 0.275 ft.
d/b	nondimensional sting diameter, 0.1375
M	Mach number
Rn	Reynolds number, based on c_{bar}
r_{le}	streamwise leading-edge radius
S	wing reference-area, 2.1445 ft^2
t	wing thickness, 0.875 in.
t/c_{bar}	nondimensional wing thickness, 0.051
w_{ls}	NTF test section width, 8.2 ft.
x,y,z	Body-axis Cartesian coordinates
x_v	Longitudinal distance to vortex origin

α	angle of attack
η	percent semispan location, 2y/b
Λ_{le}	wing leading-edge sweep
λ	wing taper ratio, c_t/c_r, 0.

INTRODUCTION
High performance military aircraft performance requirements often dictate the use of swept slender wings in order to meet a number of their multi-mission requirements. Recently, the requirement for low observability has added new constraints to vehicle shaping which results in a further compromise with aerodynamics and other disciplines to achieve a successful aircraft design. In particular, this constraint can drive the wing leading edge radius to values smaller than what might otherwise be employed for purely aerodynamic considerations.

The swept slender wing is conducive to separation-induced leading-edge vortex flows. Considerable study of this phenomena has been performed for slender wings with sharp leading edges.[1-7] However, the presence of a finite leading edge radius considerably alters the separation properties of this vortex flow and has received much less attention than the sharp-edged case. One particular complication for the blunt leading edge is the occurrence of Reynolds number sensitivities, especially as regards separation onset and progression of the primary vortex. Using a sharp leading edge eliminates this particular Reynolds number sensitivity.

Reynolds number effects tend to be fairly specific to flow domain, vehicle class, and even configuration application (e.g., cruise vs. high lift) because of the complexities associated with viscous/inviscid or viscous/viscous flow physics interactions. This is especially so for flows involving the onset and progression of separation or other state changes, like transition. Several summary papers are provided in the references

*Senior Research Engineer, Configuration Aerodynamics Branch, Associate Fellow, AIAA

that address these issues for transports[8-10] and fighters[10-12] as well as for basic airfoils[13] and forebodies.[14]

The present investigation is directed at quantifying the effects of leading-edge bluntness and Reynolds number on the onset and progression of leading edge separation for a 65° delta wing. Selected results are presented from an extensive test[15-18] performed in the NTF. The data selected for this analysis were obtained at a free-stream Mach number of 0.4 and at Reynolds numbers of 6 million and 60 million based on the wing mean aerodynamic chord. At this Mach number no data were available at intermediate Reynolds numbers. Although this precludes a detailed analysis of Reynolds number trends, the data do provide insight to the aggregate aerodynamic differences between what would be fairly typical wind-tunnel conditions (6 million) and flight values (60 million) of Reynolds number.

Analysis is primarily focused on detailed static surface pressure distributions, and inferences regarding the onset and progression of leading-edge vortex separation are made. A brief description of the experimental program follows.

EXPERIMENTAL PROCESS
The delta wing program was one of the original fundamental tests planned for the NTF. It was envisioned that these data would serve as a good initial assessment of leading-edge bluntness and Reynolds number effects on vortex flow aerodynamics, and that subsequent test programs could be launched based upon analysis of these findings. It was also envisioned that these data would be useful for calibrating computational fluid dynamics predictions of these aerodynamics. To help facilitate numerical analysis, the entire wing and near-field sting were developed as fully analytical surfaces, continuous through second derivative and, hence, curvature.

National Transonic Facility
The NTF can be operated at Mach numbers ranging from 0.1 to 1.2, at total pressures from 1.1 to 8.8 atmospheres, and at total temperatures from around 120° F down to -250° F, the cryogenic temperatures being achieved through the evaporation of injected liquid nitrogen. The test section is 8.2 feet square and approximately 25 feet long. An aerial view along with the basic facility circuit is shown in Figure 1.

a) Facility aerial view
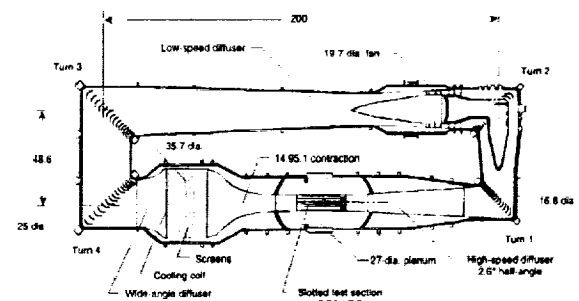
b) Facility circuit.
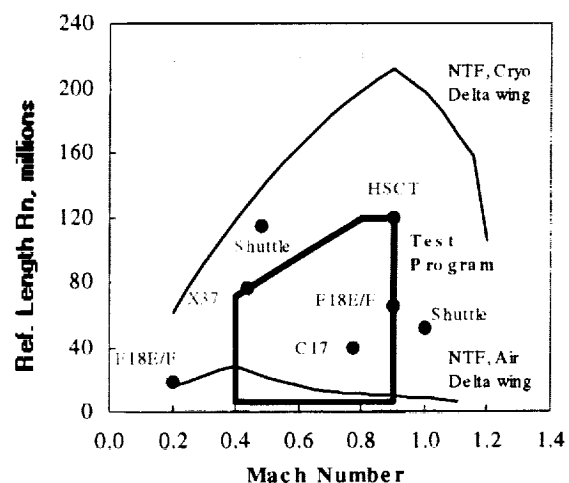Fig. 1 - The National Transonic Facility, NTF.

Fig. 2 – Facility Envelopes.

Some overall Mach-Reynolds number facility envelopes are presented in Figure 2 for NTF. The two facility envelopes represent maximum Reynolds number capability, for both the air and

cryogenic modes of operation, and the reference length for these envelopes is the delta wing mean aerodynamic chord, 1.4297 ft. The nominal test condition bounds for the delta wing program are also shown. In addition, some operating conditions for a variety of slender vehicles as well as a typical High-Wing Military Transport (C-17) are also shown for reference.

As shown in Figure 2, the range of the delta-wing test program includes sufficiently high Reynolds number conditions for the data to be relevant to full-scale vehicle flows. Of comparable importance to the high Reynolds number capability, though, is the ability in NTF to independently vary one free stream parameter, such as Reynolds number, while holding two other free stream parameters, such as Mach number and dynamic pressure, constant. This capability can be exploited to eliminate certain pseudo-Reynolds-number effects[10], and thereby allow pure Reynolds number or compressibility effects to be extracted with an experimental program.

Pure aeroelastic effects could also be determined in a similar manner. For tests where aeroelasticity is not a concern, the temperature and pressure capability of the facility can be traded off to either save time or consumables in achieving high-Reynolds-number test conditions. Addition facility details can be found among Refs. 19-22.

Wind Tunnel Model
The model was a full-span delta wing mounted on an offset sting to obtain the desired angle of attack range. The model was an uncambered flat plate with special consideration given to the leading and trailing edges as will be described subsequently. As mentioned previously, the delta-wing geometry was fully analytical with continuity through second derivative and, hence, curvature. A photograph of the model is shown in Figure 3, and some overall configuration dimensions are included in the nomenclature.

The wing was designed for a series of interchangeable leading edge components. The leading edge contours (Figure 3b) were defined with an NACA-like airfoil polynomial[23] for four values of leading-edge bluntness, r_{le}/c_{bar}, that were 0 (sharp), 0.0005, 0.0015, and 0.0030. These leading-edge contours matched the flat-plate wing
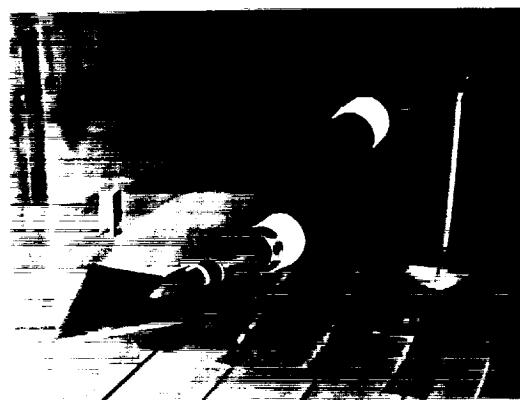
a) Delta-wing in NTF
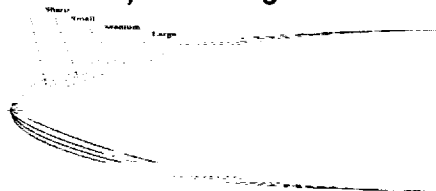
b) Airfoil leading-edge contours (not to scale)
Fig. 3 – NTF delta wing.

at 15% of the root chord and were constant spanwise to match the flat-plate central portion of the wing. This leading-edge contour region is also indicated in Figure 4.

The flat-plate portion of the wing extended back to 90% root chord, and the nondimensional wing thickness, t/c_{bar}, was 0.051. A flat plate was chosen not only for its simplicity, but also to facilitate future non-intrusive boundary-layer measurements. Aft of 90% root chord the wing thickness smoothly diminished to a sharp trailing edge. The model was fabricated from VascoMax C-200, which is suitable for cryogenic testing. The model was polished to a surface finish of 8 micro inches.

The delta wing is a very basic aerodynamic shape, and for the NTF program the wing was made as thin and simple as possible for the testing environment. The bluntness values were chosen to be on the order of values used in slender wing designs. For example, the NACA 6-series of airfoils[23] have been used as a basis for slender wing design, and the NACA 65A006 airfoil (six percent thick versus 5.1 percent for the NTF delta wing) has a leading-edge bluntness, r_{le}/c, of 0.0023. As a second basis of comparison, the

delta-wing bluntness values were contrasted with those from two somewhat dated but highly-swept-wing aircraft, the F-106B ($\Lambda_{le} = 60°$) and the F-16XL ($\Lambda_{le} = 70°$), that have been used for NASA flight test programs.[24-25] Normalized by c_{bar}, the F-106 bluntness varies between 0.0020 and 0.0005 whereas the F-16XL bluntness is very close to 0.0005 with less spanwise variation. Current design guidelines tend toward small values of bluntness as well as generally small spanwise variations of the bluntness.

The support mechanism was a ten degree offset sting designed to position the model at the center of the test section over the angle of attack range investigated. The offset allowed for testing at angles of attack of nominally –2 to 28 degrees. The near-field sting was an uncambered body of revolution that emerged symmetrically from the wing slightly aft of the 60% root chord station. It was also a fully analytical surface based upon the same functions used to represent the leading-edge shapes. The sting diameter was designed to be the minimum allowable to accommodate the design load of 6500 pounds normal force and to also house necessary instrumentation leads.

Instrumentation
The model was instrumented with 183 static surface orifices as illustrated in Figure 4. The internal diameter of the orifices was 0.010 inches. The orifice arrangement allowed for fairly good spanwise resolution at the five chordwise stations
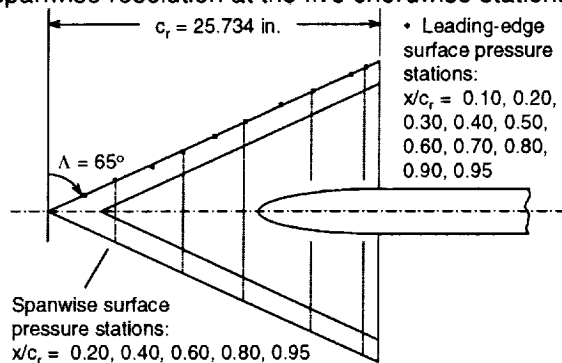

Fig. 4 – Static surface pressure stations.

(normalized by the root chord) of 0.2, 0.4, 0.6, 0.8, and 0.95. In addition, static surface pressure orifices were located every 10% root chord directly on the blunt leading edges to provide measurement of the onset and progression of leading-edge separation.

In order to avoid fuselage effects and to minimize sting interference effects, most instrumentation was situated remotely to the model. Pressure tubing was routed through the sting to electronically scanned pressure (ESP) modules. Because of the number of pressure tubes, there was no room for a conventional force balance. However, normal force and pitching moment quantities were measured through a novel gauging arrangement with the near-field sting. Balance accuracy gauging on the sting itself allowed for the measurement of these quantities. Unfortunately, there was no similar means to obtain axial-force measurements.

Angle of attack was determined from the combination of arc-sector setting and calibrated sting-bending effects using the sting gauges just mentioned. On-board inclinometers were too large to include in this thin-wing model.

Test Conditions and Procedures
The tests were conducted in 1991 and included Mach numbers ranging from 0.4 to 0.9. Reynolds number was varied from 6 million to 120 million in such a way as to facilitate analysis at Reynolds numbers based on either the wing mean aerodynamic chord or the wing leading-edge radius. A representative matrix of test conditions
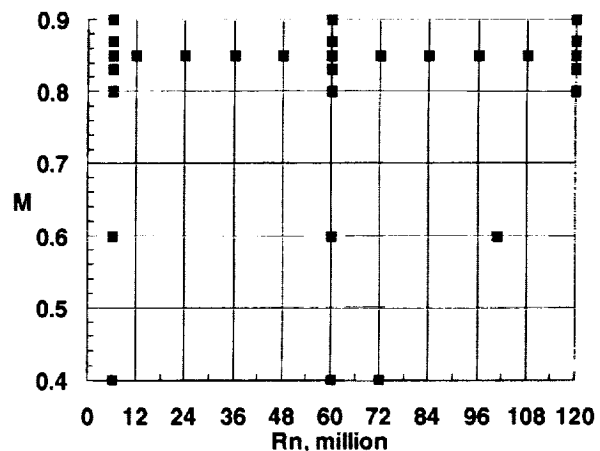

Fig. 5 – Representative test matrix.

is shown in Figure 5 for the medium leading-edge bluntness wing. Not all of these conditions were replicated for every leading edge due to resource limitations. As can be seen from this figure, the

primary emphasis of the test program was on transonic Reynolds number effects.

Data were obtained at only two total temperatures, nominally 120° F and –250° F. Total pressure was varied nominally between 1.1 and 5.3 atmospheres to obtain the desired free stream test conditions. Because aeroelastic effects for this model were negligible, this approach was adopted to save occupancy time and reduce liquid nitrogen consumption.

No artificial transition strips were affixed to the model. It was anticipated that the flow would naturally be turbulent over the Reynolds numbers tested. Moreover, there were no clear transition-strip test techniques for these vortex flows.

A number of potential pseudo-Reynolds-number effects were considered and minimized in the design of the experiment. Calculations indicated that aeroelastic deformation would be small due to the low aspect ratio of the wing, the thickness of the wing, and the stiffness of the material. The 8-microinch surface finish was sufficient for the model to be hydraulically smooth over the range of conditions tested.

Wind tunnel wall interference was believed to be negligible due to the slotted test section and the relative size of the delta wing to the test section $(b/w_{ts} = 0.244)$. In addition, test section walls, model support walls, and reentry flaps were all set to minimize wall effects based upon facility guidelines. The model support mechanism was designed to keep the model centered in the test section. This essentially eliminated pseudo-angle-of-attack effects associated with the model traversing the test section flow and/or getting too close to the ceiling at high angles of attack.

RESULTS

Results will be presented first to contrast the sharp and blunt-edged vortex flows for a fixed angle of attack. This will be followed by an analysis contrasting low and high Reynolds number flows for the medium leading-edge bluntness. Finally, effects for the other bluntness values will be presented. Because the analysis is focused on static surface pressures, a brief review of the relation of these pressures to the off-body vortical structures is presented.

Basic flow structures
Many studies of sharp-edged vortex flows from slender wings have been published. Perhaps the best known results are due to Hummel who reported extensive measurement and analysis of the flow about an aspect ratio one delta wing. In that study the leading edge was sharp.

A figure from Hummel's work[2] is repeated as Figure 6 below. In this figure, the spanwise pressure distribution is shown along with a sketch of the off-body vortical structures. The data show the suction peak associated with the spanwise flow acceleration induced by the primary leading-edge vortex. Outboard of the suction peak there is an adverse spanwise pressure gradient, and this causes the wing boundary-layer flow to separate and form a smaller secondary vortex of opposite sign. The sketch represents laminar secondary separation; for the turbulent case the pressures between the secondary separation and the leading edge tend to be relatively flat and less negative than the primary suction peak.[2]
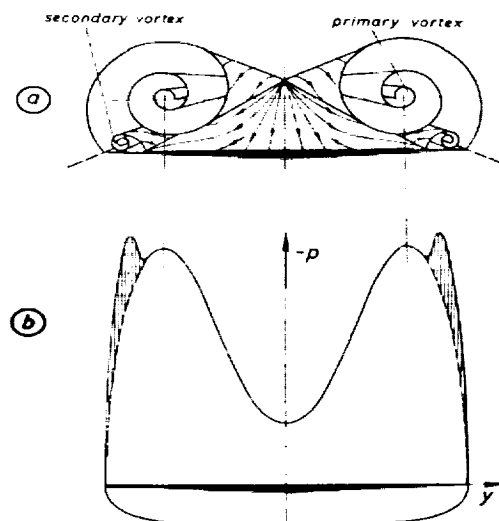

Fig. 6 - Basic vortex flow structures and pressures. From Hummel.[2]

The geometry of the sharp-edged vortex flow is fairly conical. Peak suction pressures will occur near the same percent semispan for the entire wing. The value of the peak suction will be non-conical, and some vortex curvature effects will be manifested near the trailing edge. The blunt leading edge fundamentally alters this flow.
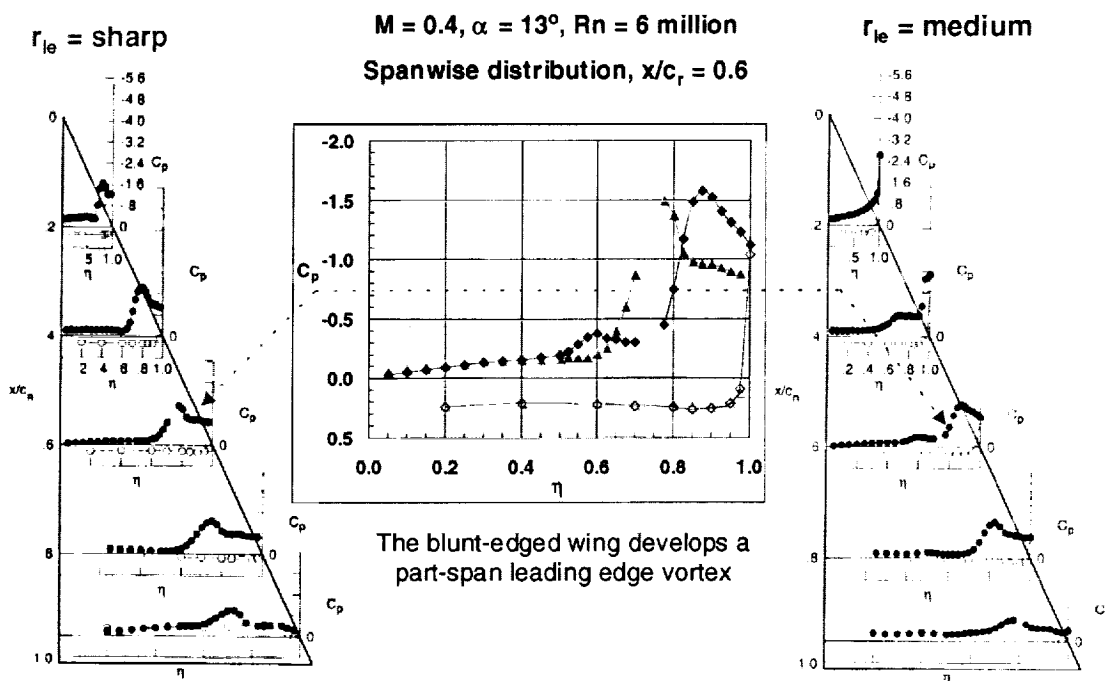
Fig. 7 - Comparison of spanwise pressure distributions for sharp-edged and blunt wings.

Bluntness and Reynolds number Effects

The flows for the sharp and medium leading-edge bluntness configurations are compared first at the same angle of attack (13°) and the conventional wind tunnel Reynolds number (6 million). See Figure 7. The sharp-edge flow for this 65° delta wing bears many expected similarities to the features just described from Hummel's work for turbulent secondary separation. The measurements show the leading-edge vortex pressures manifested over all pressure stations.

The blunt edge flow differs from the sharp edge case in several respects. First, it is clear that the blunt edge has delayed separation along the leading edge. At the forward most longitudinal station (x/c_r = 0.2) the spanwise pressures clearly show an attached-flow distribution. At the 80% station the spanwise pressures show a fairly typical leading-edge vortex pressure distribution for turbulent secondary separation. A part-span vortex has formed on the blunt leading edge with the origin somewhere between the 20% and the 60% root chord stations.

There is a second and subtler difference between these two cases. In the comparison plot of the sharp and blunt spanwise pressures at the 60% station, the data for the blunt edge show local small suction peak approximately at the 60% semispan location. This is inboard of the primary vortex suction peak. The pressures at the 40% chord station also show an altered pressure distribution in the 60% to 80% span region from what would be expected for purely attached flow. In this region the pressures are very flat.

The implication of these pressures is toward a different separation structure for the blunt edge. These pressures would be consistent with the existence of two co-rotating leading edge vortices being generated from the blunt leading edge. By this conjecture, the first primary vortex would originate somewhere aft of the 20% chord station, would be relatively weak, and would shed inboard on the wing. A second primary vortex separation would then occur with the more familiar pressure signature attributes.
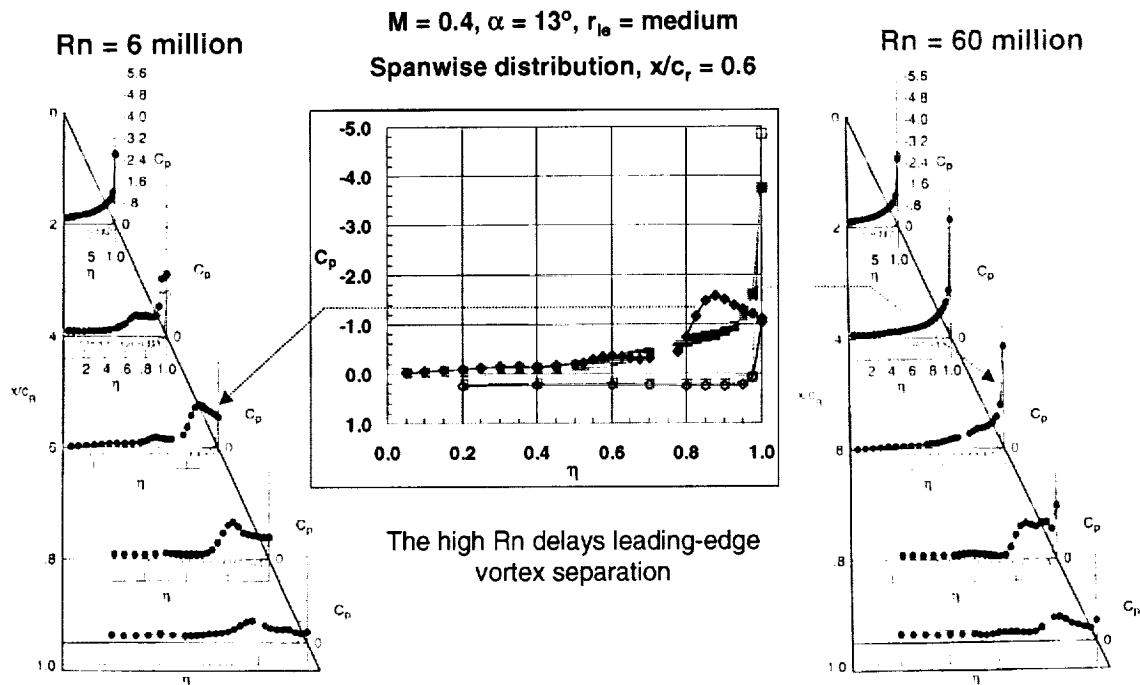
Fig. 8 - Reynolds number effect on blunt leading edge separation – spanwise pressure distributions.

Although the multiple co-rotating vortices are strictly a conjecture to the measured pressure distributions, they certainly can and do occur on wings with relatively uniform leading-edges.[24,26] This conjecture for the delta wing flow could be resolved with surface flow visualization studies.

The effect of Reynolds number is next considered for the same bluntness and angle of attack. A comparison of the low and high Reynolds number results is presented in Figure 8. The high Reynolds number results demonstrate that the origin of the leading-edge vortex separation has been shifted aft by at least 20% root chord. The subsequent vortex also resides closer to the leading edge.

The high Reynolds number data show an attached-flow pressure distribution at the 40% chord station. At the 60% chord station the data show a slight plateau just outboard of 80% span. (See the comparison plot of the low and high Reynolds number data in the above figure.) This may be an indication of the initial or weak leading-edge vortex separation just discussed for the low Reynolds number data. By 80% chord the pressures show a somewhat more familiar leading-edge vortex separation. However, these data show a second suction peak outboard of what would be expected to be the primary vortex suction peak. The origin for this second peak is unclear.

The high Reynolds number flow has shifted the origin of the leading-edge vortex separation aft on the wing at this angle of attack. The extent of this effect will be examined next in terms of leading-edge pressure distributions and angle of attack effects.

The blunt-edges for this delta wing included pressure instrumentation directly at the leading edge every 10% root chord. These pressure taps were intended to provide an indication of the forward progression of the leading edge vortex separation with increasing angle of attack.
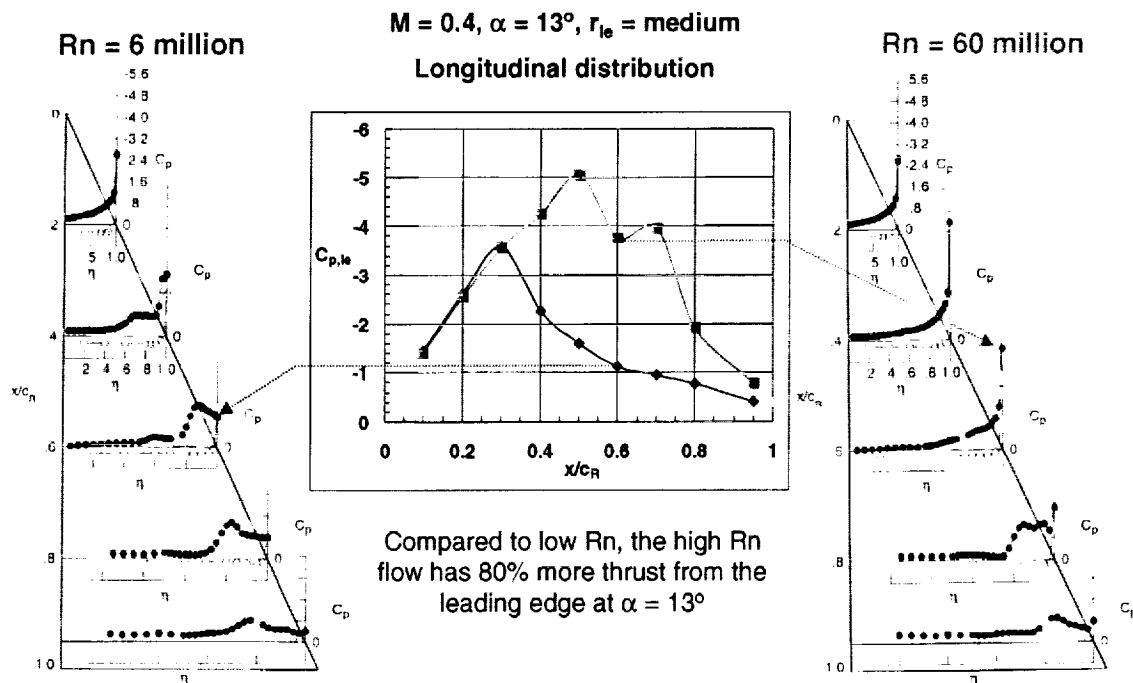
Fig. 9 - Reynolds number effect on blunt leading edge separation – leading-edge pressure distributions.

The Reynolds number effect on leading-edge separation is more clearly seen by contrasting these leading-edge pressures at the two conditions just discussed. The same surface pressure distributions from Figure 8 are repeated in Figure 9 but the inset pressure comparison is now for the leading-edge pressures. These pressures are plotted against percent root chord, which is identical to fractional distance down the leading edge.

For the low Reynolds number data, the pressures show an attached flow trend back to 30% chord. By 40% chord the leading-edge suction pressure has collapsed from what would be expected theoretically, and it is inferred that at this station the flow has separated at the leading edge. This result is consistent with the prior observations regarding the low Reynolds number spanwise pressure distribution at the 40% chord station. The evidence for separation is however more compelling in the leading-edge pressure data than in the upper-surface pressure data.

The high Reynolds number data show the flow to be attached back to 50% chord or so. Aft of this station the data show a longitudinal oscillation in the leading-edge pressure at 60% chord and the source of this is unclear. Once again the trends in leading-edge pressures are consistent with those already discussed for the upper surface pressures. Reynolds number effects extend over the aft 70% of the wing.

The pressures down the leading edge are an indication of the leading-edge suction being developed in the wing-chord plane. The low and the high Reynolds number leading-edge pressure distributions were integrated down the leading edge to estimate the Reynolds number effect on aggregate leading-edge suction. The results indicate that the high Reynolds number case develops approximately 80% more suction than the low Reynolds number case at this angle of attack.
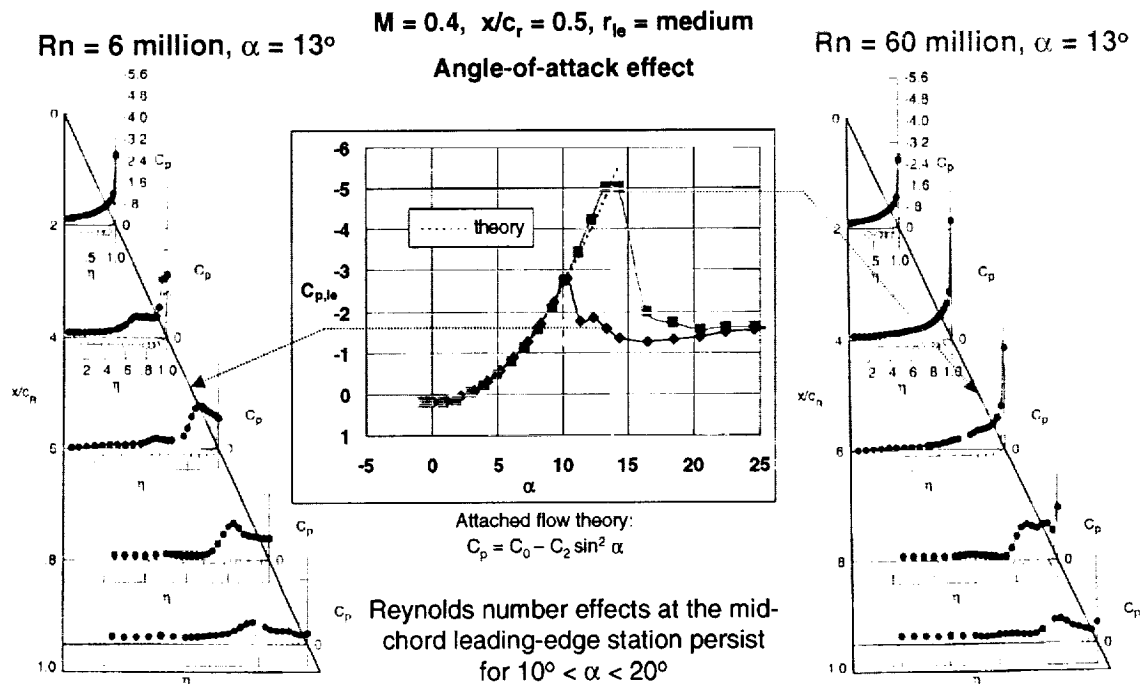
M = 0.4, x/c_r = 0.5, r_le = medium

Angle-of-attack effect

Rn = 6 million, α = 13°

Rn = 60 million, α = 13°

Attached flow theory:
$$C_p = C_0 - C_2 \sin^2 \alpha$$

c_p Reynolds number effects at the mid-chord leading-edge station persist for 10° < α < 20°

Fig. 10 - Reynolds number effect on blunt leading edge separation – angle of attack effect.

Thus far the analysis of Reynolds number effects has been focused on an angle of attack of 13°. The Reynolds number effects are by no means restricted to this angle.

The leading-edge pressures were shown with the previous figures to provide a useful measure of the local state (attached versus separated) of the flow. These pressures are now used to assess angle-of-attack effects between the low and high Reynolds number flows.

In Figure 10 the inset comparison plot is for the leading edge pressure at the 50% chord station. This one pressure is plotted against angle of attack for the low and the high Reynolds number conditions. The low Reynolds number data show the flow to separate at this station between 10° and 11°. For the high Reynolds number flow, the flow stays attached at this station to approximately 13°. However, significant differences between the low and high Reynolds number flows are manifested for angles of attack ranging between 10° and 20°. The spanwise

pressure distributions are repeated for the 13° angle of attack case to relate the previous analysis to the angle-of-attack trends.

The figure also shows the expected theoretical trend for attached flow pressures. The coefficients for the theory were obtained from a linear least-squares fit of the data at low angles of attack. The attached flow theory models the experimental pressures very well through higher angles of attack up to the condition for which the flow separates. The departure of the experimental pressures from the attached flow trend is very sudden for both the low and high Reynolds number conditions.

The longitudinal analysis of the leading edge pressures presented in Figure 9 provided one means to identify a longitudinal position of leading-edge separation for a fixed angle of attack. The results of Figure 10 present an alternate approach of identifying the angle of attack at a given longitudinal station that the flow separates. Because of the relatively fine
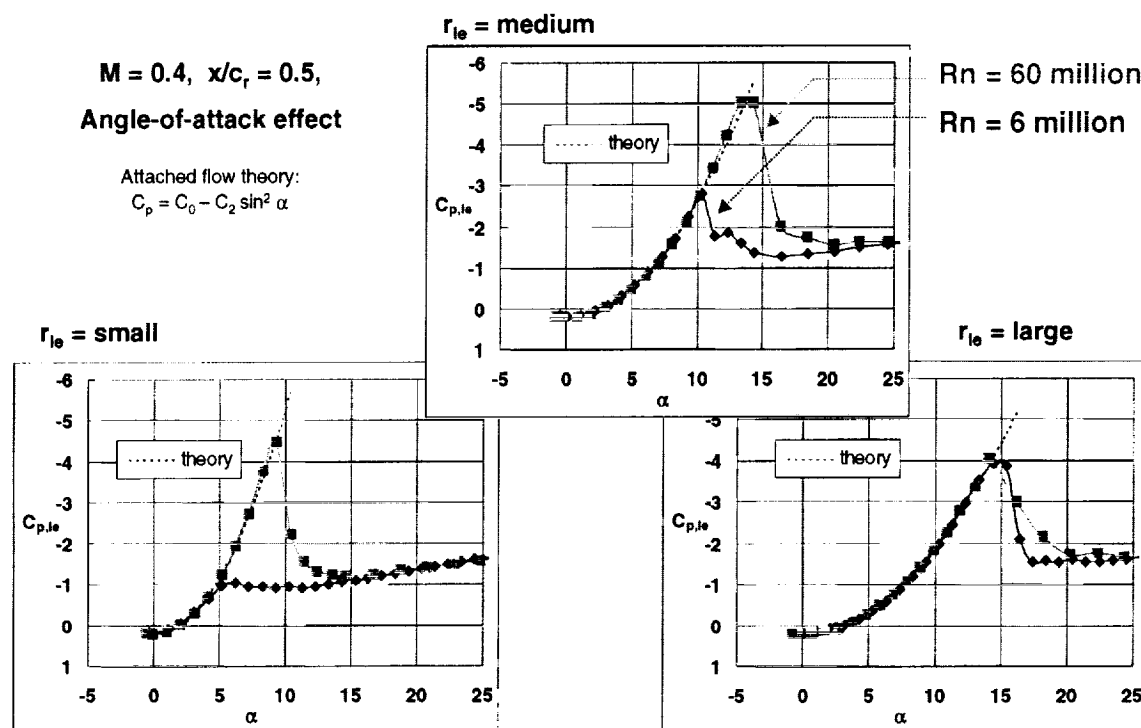
Fig. 11- Reynolds number effects for three leading-edge bluntness values.

increments in angle of attack, this latter approach is preferable for mapping out the progression of separation up the leading edge.

Thus far the data for the intermediate bluntness has demonstrated substantial Reynolds number effects. These have been shown for an extensive longitudinal region of the wing (at fixed angle of attack) and for a substantial angle of attack range (for a fixed longitudinal leading edge pressure). The leading-edge pressure has also been shown to be representative of larger-scale separation effects.

The results discussed thus far are also manifested for the small and large leading-edge bluntness. Leading-edge pressures similar to those just discussed are presented in Figure 11 for all three bluntness. The results show that, for the small leading-edge bluntness the low

Reynolds number flow separates at this station at approximately 5°. The high Reynolds number data remain attached at this station up to an angle of attack of 9°, and significant differences between the low and the high Reynolds number data are manifested over angles of attack ranging from 5° to 15° at this station.

For the large leading-edge bluntness both the low and the high Reynolds number data indicate flow separation at approximately 14°. There are some differences between the low and high Reynolds number data over an angle of attack range of 14° to 20°, but these differences are not as great as those observed for the other two blunt leading edges. This bluntest leading edge seems to exhibit different trends from the other two blunt leading edges.

M = 0.4, x/c_r = 0.5,

Angle-of-attack effect

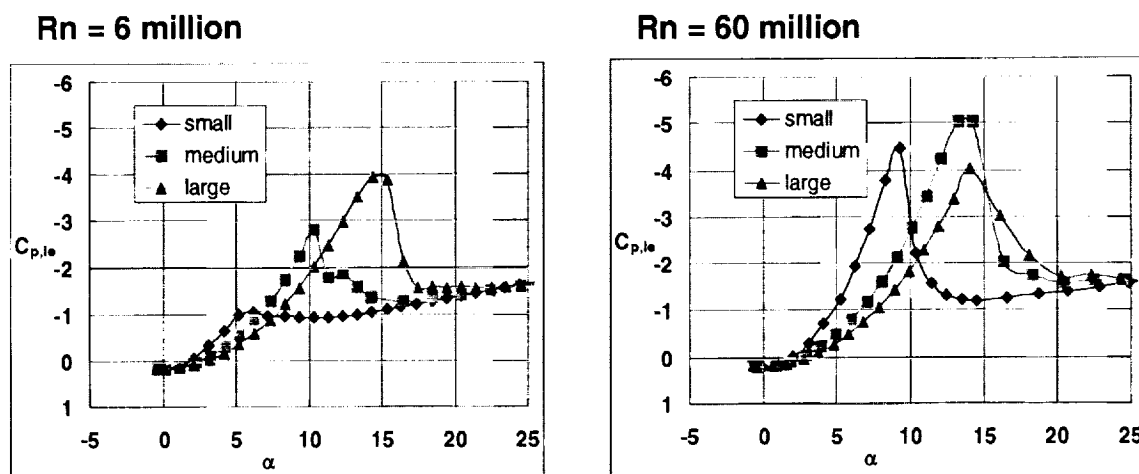### Rn = 6 million

Rn = 60 million

Fig. 12 - Leading-edge bluntness effects at low and high Reynolds number.

The results of the previous figure are presented in Figure 12 to directly contrast bluntness effects at the low and high Reynolds numbers tested. At the low Reynolds number condition, the data show a fairly continuous trend in the peak pressure that corresponds to the onset of local separation. In particular, this low Reynolds number trend shows that the bluntest leading edge delayed separation at this mid-chord station by 5° as compared to the moderate leading-edge bluntness.

However, at the high Reynolds number condition, the medium leading edge bluntness evidences attached flow up to 13° or so, and the large bluntness shows no further effect as regards the delay of local flow separation.

The results discussed with the medium leading-edge bluntness demonstrated a link between the peak leading-edge suction and the onset of local

leading-edge separation. The results from Figure 12 indicate that this effect could be used to identify trends in leading-edge separation.

Figures 13 and 14 present this leading-edge pressure analysis for three longitudinal stations at the low and high Reynolds number conditions, respectively. The data show that bluntness and Reynolds number effects are manifested at these other stations as well.

Overall, the results show similar trends with regard to the onset of separation. The peak leading-edge suction pressure can be used as a gauge to identify the progression of separation up the leading edge as angle of attack is increased. This analysis was performed for the full M = 0.4 data base from the NTF experimental program and the results are summarized in Figure 15.

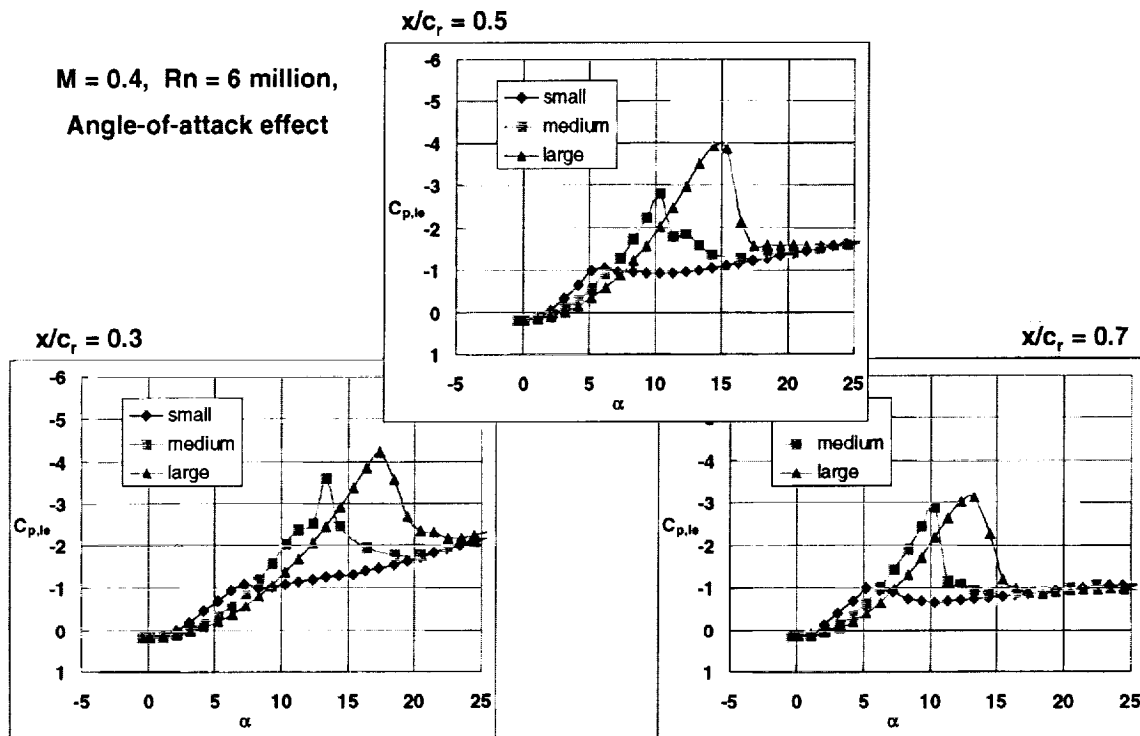x/c_r = 0.5

M = 0.4, Rn = 6 million,
Angle-of-attack effect

x/c_r = 0.3

x/c_r = 0.7

Fig. 13 - Longitudinal variation of bluntness effect, low Reynolds number.

x/c_r = 0.5

M = 0.4, Rn = 60 million,
Angle-of-attack effect

x/c_r = 0.3

x/c_r = 0.7
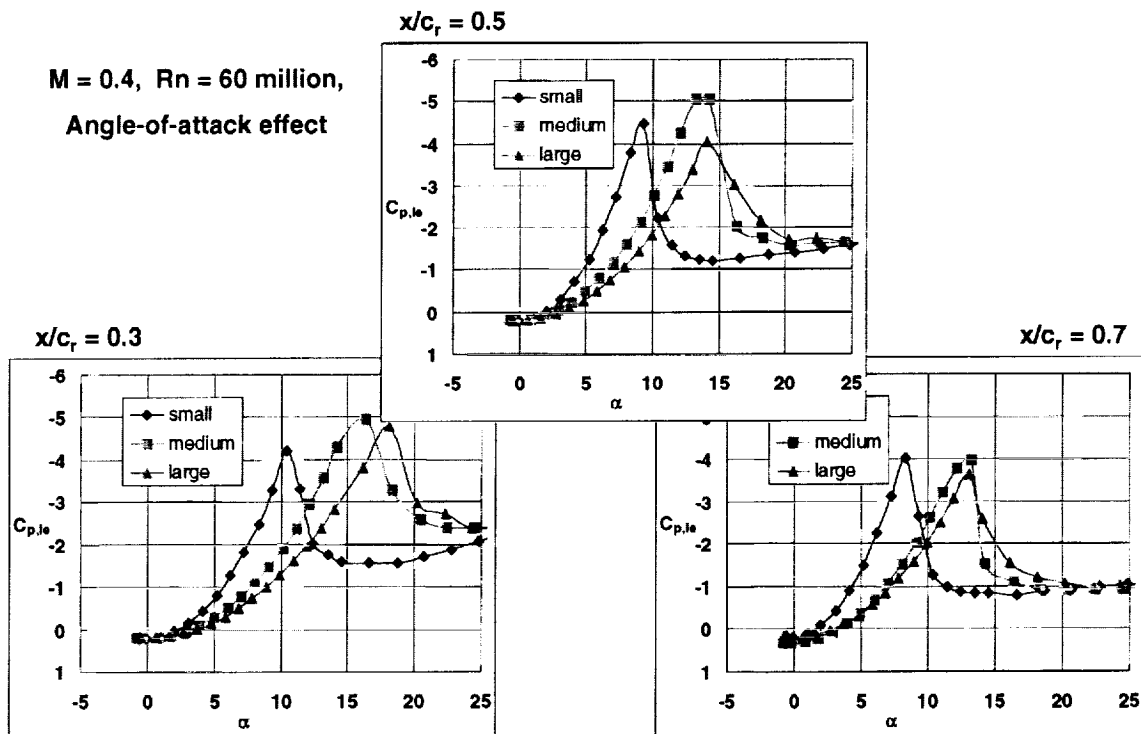
Fig. 14 - Longitudinal variation of bluntness effect, high Reynolds number.

American Institute of Aeronautics and Astronautics

The data of Figure 15 show the deferred onset and subsequent progression of leading-edge vortex separation with angle of attack for the three blunt edges at the low and the high Reynolds numbers. At low Reynolds number the small and medium bluntness data are offset in angle of attack by approximately 4°. Both of these leading edges show a rapid progression of the separation up to about 40% chord after which the progression is more gradual. The blunt leading edge shows a more gradual progression of leading edge separation.

At high Reynolds numbers (Figure 15b) the onset of separation is about 2° higher in angle of attack than the low Reynolds number data for the small and medium leading edges. It also seems as if the progression of separation up the leading edge was slightly more gradual at high Reynolds numbers. The bluntest leading edge showed smaller differences due to Reynolds number.

FINAL REMARKS
An analysis of Reynolds number and leading-edge bluntness effects on the flow about a 65° delta wing has been presented. Analysis was focused upon data obtained at a free stream Mach number of 0.4 out of an extensive data set generated in the NTF.

The results of this analysis show significant bluntness effects on the onset and progression of separation-induced leading-edge vortex flows. The data also demonstrate extensive differences at a low (6 million) and a high (60 million) Reynolds number. These two values are comparable to typical ground-based wind tunnel conditions and flight conditions, respectively. Examples were shown where Reynolds number differences extended over 70% of the wing (at a fixed angle of attack) and over a 10° angle-of-attack range (at fixed positions).

The data also imply that the character of the blunt edge separation could be different from the sharp edge case. Static surface pressure distributions were used to conjecture the presence of two co-rotating leading-edge vortices on the wing. This feature could be resolved with additional testing that could be as simple as surface flow visualization studies.
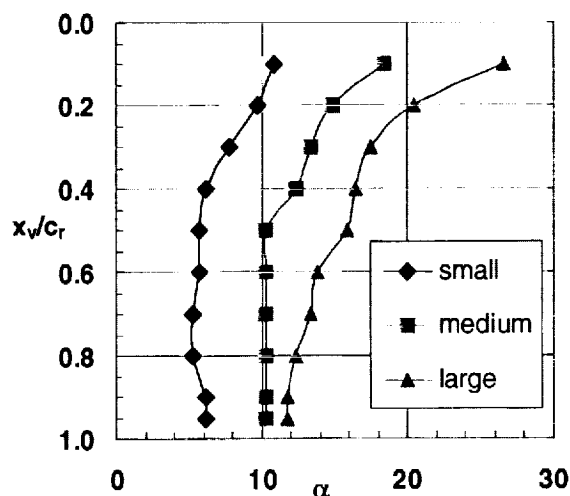
a) Rn = 6 million
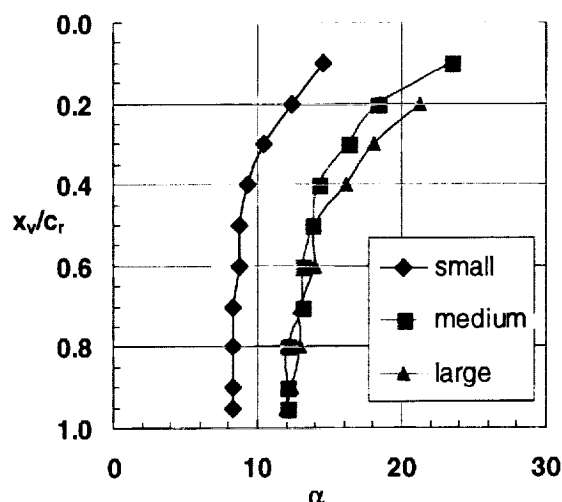
b) Rn = 60 million

Fig. 15 - Progression of leading-edge vortex separation.

The measurements also demonstrated the utility of leading-edge pressures for inferring the origin of blunt leading-edge vortex separation. Trends from these leading-edge pressures were consistent to those observed from upper surface pressures.

Additional testing with this delta wing configuration would be very useful. Both surface and off-body flow visualization data

would add great insight to the overall topology of this vortex flow. Boundary layer and off-body flow field measurements could also add greatly to the understanding of the surface flow properties as well as the leading-edge vortex flow field including breakdown effects. Six-component force and moment data would also be a welcome adjunct to the data set. Although Reynolds number effects are not negligible, many experimental contributions could be performed at conventional Reynolds numbers. Low-speed data at intermediate Reynolds numbers to those presented would also be helpful for analyzing Reynolds number trends or scaling concepts.

The data from this experiment could also provide a useful challenge for Computational Fluid Dynamics (CFD) methods. It would be most instructive to see if the blunt leading-edge vortex flow could be predicted with CFD. Predictions for Reynolds number and bluntness effects would be would be of interest as well.

ACKNOWLEDGMENT

REFERENCES

[1]Polhamus, E. C., "A Concept of the Vortex Lift of Sharp-Edged Delta Wings Based on a Leading-Edge Suction Analogy," NASA TN D-3767, 1966.

[2]Hummel, D., "On the Vortex Formation Over a Slender Wing at Large Incidence," AGARD CP-247, Paper No. 15, January 1979.

[3]Smith, J. H. B., "Improved Calculations of Leading-Edge Separation from Slender Delta Wings". RAE TR-66070, 1966.

[4]Hemsch, M. J., and Luckring, J. M., "Connection Between Leading-Edge Sweep, Vortex Lift, and Vortex Strength for Delta Wings," AIAA J. Aircraft, Vol. 27, No. 5, May 1990.

[5]"High Angle of Attack Aerodynamics," AGARD CP-247, January 1979.

[6]"Aerodynamics of Vortical Type Flows in Three Dimensions," AGARD CP-342, July 1983.

[7]"Vortex Flow Aerodynamics," AGARD CP-494, July 1991.

[8]Lynch, F. T., "Commercial Transports – Aerodynamic Design for Cruise Performance Efficiency," Transonic Aerodynamics, Progress in Astronautics and Aeronautics, Vol. 81, 1982.

[9]Goldhammer, M. E., and Steinle, F. W., Jr., "Design and Validation of Advanced Transonic Wings Using CFD and Very High Reynolds Number Wind Tunnel Testing," 17th ICAS Congress, September 1990.

[10]Elsenaar, A., Binion, T. W. Jr., and Stanewsky, E., "Reynolds Number Effects in Transonic Flow," AGARDograph AG-303, December 1988.

[11]Haines, A. B., "Scale Effects on Aircraft and Weapon Aerodynamics," AGARDograph AG-323, July, 1994.

[12]Henderson, W. P., "Study of Various Factors Affecting Drag Due to Lift at Subsonic Speeds," NASA TN D-3584, October 1966.

[13]Polhamus, E. C., "A Survey of Reynolds Number and Wing Geometry Effects on Lift Characteristics in the Low Speed Stall Region," NASA CR-4775, June 1996.

[14]Polhamus, E. C., "A Review of Some Reynolds Effects Related to Bodies at High Angles of Attack," NASA CR-3809, August 1984.

[15]Chu, J., and Luckring, J. M., "Experimental Surface Pressure Data Obtained on 65° Delta Wing Across Reynolds Number and Mach Number Ranges. Volume 1 – Sharp Leading Edge," NASA TM-4645, February 1996.

[16]Chu, J., and Luckring, J. M., "Experimental Surface Pressure Data Obtained on 65° Delta Wing Across Reynolds Number and Mach Number Ranges. Volume 2 – Small Leading Edge," NASA TM-4645, February 1996.

[17]Chu, J., and Luckring, J. M., "Experimental Surface Pressure Data Obtained on 65° Delta Wing Across Reynolds Number and Mach Number Ranges. Volume 3 – Medium Leading Edge," NASA TM-4645, February 1996.

[18]Chu, J., and Luckring, J. M., "Experimental Surface Pressure Data Obtained on 65° Delta Wing Across Reynolds Number and Mach Number Ranges. Volume 4 – Large Leading Edge," NASA TM-4645, February 1996.

[19]Wahls, R. A., "The National Transonic Facility – A Research Retrospective," AIAA Paper 01-0754, January 2001.

[20]Luckring, J. M., "An Overview of National Transonic Facility Investigations for High Performance Military Aerodynamics" AIAA Paper 01-0906, January 2001.

[21]Fuller, D. E., "Guide for Users of the National Transonic Facility," NASA TM-83124, 1981.

[22]Foster, J. M., and Adcock, J. B., "Users Guide for the National Transonic Facility Research Data System," NASA TM-110242, April 1996.

[23]Abbott, I. H., and Von Doenhoff, A. E. "Theory of Wing Sections," Dover Publications, Inc., 1959.

[24]Lamar, J. E., Brandon, J. M., Stacy, K, Johnson, T. D., Jr., Sevrence, K., and Childers, B. A., "Leading-Edge Vortex System Details Obtained on F-106B Aircraft Using a Rotating Vapor Screen and Surface Techniques," NASA TP-3374, November 1993.

[25]Lamar, J. E., Obara, C. J., and Fisher, B. D., "Flight, Wind-Tunnel, and Computational Fluid Dynamics Comparison for Cranked Arrow Wing (F-16XL-1) at Subsonic and Transonic Speeds," NASA TP-2001-210629, February 2001.

[26]Campbell, J. F., and Chambers, J. R., "Patterns in the Sky," NASA SP-514, 1994.